Neutron diffraction study of the α- to β- phase transition in BaD_2 under high pressure

Christopher J. Ridley, Nicholas P. Funnell,
Craig L. Bull and Holger Kohlmann

Published version information

Citation: CJ Ridley et al. "Neutron diffraction study of the α- to β- phase transition in BaD_2 under high pressure." Solid State Communications, vol. 318 (2020): 113965.

DOI: 10.1016/j.ssc.2020.113965

Neutron diffraction study of the α- to β- phase transition in BaD_2 under high pressure

Christopher J. Ridley[a,*], Nicholas P. Funnell[a], Craig L. Bull[a] and Holger Kohlmann[b]

[a]ISIS Neutron and Muon Source, Rutherford Appleton Laboratory, Chilton, Didcot OX11 0QX, United Kingdom
[b]Institut für Anorganische Chemie, Universität Leipzig, Johannisallee 29, 04103 Leipzig, Germany

ARTICLE INFO

Keywords:
High-pressure
Neutron diffraction
Ionic hydride
Alkali-earth hydride
First-order transition

ABSTRACT

We report high-pressure neutron diffraction, and Raman spectroscopy data from the α- (*Pnma*) to β- ($P6_3/mmc$) phase transition in BaD_2. The transition was observed at 2.53(5) GPa on pressure increase, and 1.65(5) GPa on pressure decrease, with a relatively narrow 0.20(5) GPa region of phase coexistence. We report the isothermal equations of state for the α-phase at 300 K and the β-phase at both 300 K and 480 K, and have calculated the entropy change through the transition. The Raman data show that a low energy Ba-vibration is seen to soften with applied pressure; DFT calculations suggest that this is predominantly due to an instability in the Ba atoms prior to the first-order transition. The shift in deuterium positions in the high-pressure phase suggest that the Wyckoff 4f-model (where one of the deuterium atoms is split between two sites) is a better fit at lower pressures, but that the model tends towards the Wyckoff 2d-model (where D1 is localised on a single site) with increased pressure. These results are used to discuss implications on the reported increases in ionic-conductivity over the transition.

1. Introduction

Metal hydrides have primarily been of interest due to their potential for efficient solid-state hydrogen storage, though three key features have prevented their widespread use; balancing the need for high gravimetric density of the material, low reversible decomposition temperatures, and fast hydrogen exchange kinetics [1]. Heavy alkali-earth hydrides, such as BaH_2, have received little attention for this due to their low gravimetric density, and high decomposition temperature. However, recently BaH_2 was found to show fast H^- ionic conductivity at elevated temperatures, with a large increase in the overall conductivity, which may lead to interesting applications in electrochemical energy storage and conversion systems [2], which has led to a renewed interest around heavy hydrides [3, 4].

The isomorphous crystal structures of the alkali-hydrides CaH_2, SrH_2 and BaH_2 were studied by Zintl and Harder [5], and were reported to be orthorhombic in symmetry, with the metal cation sitting on the 4c Wyckoff position, and the hydrogens assumed to occupy these sites also, resulting in a highly distorted $PbCl_2$-type structure. These were later corrected by Bergsma and Loopstra [6] using neutron powder diffraction data collected from both CaH_2 and CaD_2. These structural studies implied that the hydrogens lay in the same planar arrangement as the calcium ions, in a slightly distorted $PbCl_2$ type structure. Here the Ba may be described as coordinated by nine hydrogen atoms, six sitting at the trigonal vertices of a tricapped trigonal prism, and three at the centres of the adjoining rectangular faces. The trigonal faces form zigzag chains running along the *a*-axis, with neighbouring chains canted relative to each other and staggered along the *b*-axis. The structure consists of two distinct hydrogen positions, with D1 sitting on four of the six trigonal vertices (the corner-shared vertices of the zigzag network), and D2 sitting on two of the three rectangular faces (see Figure 1).

Peterson and Indig [7] were the first to identify the existence of a further phase in the simple ionic system (labelled as β-BaH_2), identified through thermal analysis, and then using X-ray diffraction at 870 K. The diffraction pattern was indexed with a body-centred cubic cell with a= 9.465 Å. Later, a high-temperature neutron diffraction study corrected this to a $P6_3/mmc$ hexagonal unit cell with a = 4.4571(2), c = 6.7230(4) Å at 883 K [2]. High pressure was used to study the material, first using *ab-initio* calculations [8], before two high-pressure phases were found experimentally using X-ray diffraction [9, 10, 11]. These were identified as a transition from the ambient *contunnite*-phase to a hexagonal-close-packed Ni_2In-phase at approximately 2.5 GPa, and then to a simple hexagonal (SH) phase at approximately 50 GPa.

More recently Zhang et al. [3] investigated the ionic transport behaviour under applied pressure, confirming that the high-temperature and high-pressure phases show the same increase in H^- conductivity. However, there is little structural information available at high pressures including accurate hydrogen positions, key to understanding the high-ionic conductivity in the material. High-pressure has the advantage over high-temperature of lower thermal displacement effects, where these are truly due to thermal motion, while neutron-diffraction provides information more dominated by the D ions in the structure. The present study considers the structural changes in BaD_2 at ambient temperature, and modest high temperatures (480 K), with a view to better understanding the nature of the transition to the β-phase, and

*Corresponding author
christopher.ridley@stfc.ac.uk (C.J. Ridley)
ORCID(s): 0000-0002-3060-9656 (C.J. Ridley); 0000-0001-6280-036X (N.P. Funnell); 0000-0002-5170-6674 (C.L. Bull); 0000-0002-8873-525X (H. Kohlmann)

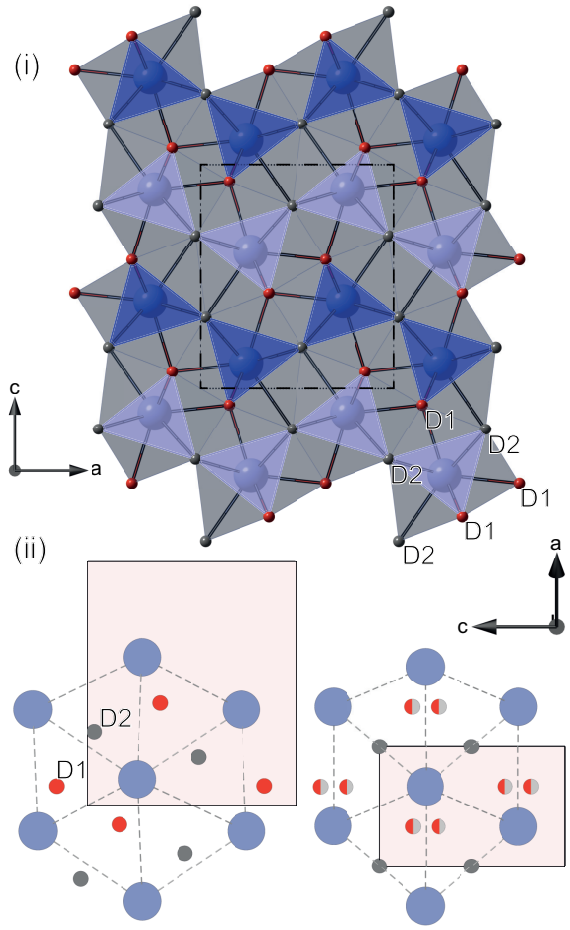

Figure 1: (i) Ambient pressure $PbCl_2$-type structure of BaD_2 as determined by powder neutron-diffraction, as viewed along [010], showing the network of ninefold Ba–D polyhedra (forming tricapped trigonal prisms). The interconnected trigonal prisms form zigzag chains along the *a*-axis, neighbouring chains canted relative to each other and staggered along *b*-axis (indicated through different colouring of the prisms). The two deuterium atoms in the unit cell are distinguished by different colouring, as labelled in the figure. The Ba and D ions sit within the (040) plane. (ii) Side-by-side structures (shown as Ba octahedra) of the α-phase at 1.92(5) GPa prior to the transition (left), and the β-phase at 2.53(5) GPa post the transition (right). The orientation is identical between the upper and lower figures, with the β-phase viewed along the [010] direction, with the partially occupied deuterium ion sites shown as half-shaded circles.

the resulting properties.

2. Experimental and calculation details

The sample was prepared through the exposure of barium metal to deuterium gas in a high-pressure autoclave. In an argon-filled glove box, pieces of barium (99.9%, Sigma Aldrich) were put in crucibles machined from hydrogen-resistant Nicrofer 5219 Nb-alloy 718, and charged with 5 MPa of deuterium gas (99.8%, Praxair) in an autoclave made from the same alloy. The autoclave was heated to a temperature of 670 K for 65 h, then slowly cooled to room temperature. The sample was stored and handled in a glove box to prevent oxide and hydroxide formation.

All neutron diffraction measurements were performed at the ISIS Neutron and Muon Source using the PEARL diffractometer [12]. High-pressure neutron powder-diffraction measurements were performed using a V4 Paris-Edinburgh press. The samples were pressurised using single-toroidal zirconia-toughened alumina anvils, and contained within a null-scattering encapsulated TiZr gasket [13]. Fully deuterated pentanes were used as a pressure transmitting medium. Sample pressure was determined using the equation of state of Pb [14]. High pressure Raman spectra were collected using a Princeton Instruments Acton SP-2500 spectrometer equipped with a 1800 g mm^{-1} grating, and a PIXIS:100B Peltier cooled CCD. The sample was excited using a 15mW narrow line width diode laser at a wavelength of 532 nm. The sample was loaded (under a controlled atmosphere) between 800 µm diameter culet diamonds used in a Merrill-Bassett cell [15], and sealed in a steel gasket, with deuterated pentanes as a pressure medium. A small ruby sphere was used to determine the sample pressure [16]. Short data sets were collected on pressure increase to determine the transition pressure, and longer exposures were recorded on pressure decrease; no differences were seen between the two apart from a shift in transition pressure.

Vibrational spectroscopy calculations were performed using the plane-wave DFT package, CASTEP 7.0.3 [17]. A plane wave cutoff energy of 750 eV was used, and k-space was sampled on a $3 \times 5 \times 3$ $Å^{-1}$ Monkhorst-Pack grid. The PW91 density functional was used with on-the-fly ultrasoft pseudopotentials [18]. The cell dimensions and contents were first relaxed via geometry optimisation, while retaining *Pnma* symmetry. The optimised volume of the unit cell, 222.518 $Å^3$, compared favourably to the experimental value, 222.103(6) $Å^3$. Convergence criteria were set as: total energy per atom 5×10^{-6} eV; maximum force 0.001 eV$Å^{-1}$; maximum displacement 5×10^{-4} Å; maximum stress 0.02 GPa. Vibrational frequencies were then calculated using the finite displacement method, with a phonon energy tolerance of 1×10^{-6} eV and a displacement amplitude of 5.3×10^{-3} Å.

3. Results and discussion

3.1. Neutron diffraction

Initially the sample was loaded into a 6 mm diameter vanadium can to confirm the ambient crystal structure, determine the level of deuteration, and to quantify the purity of the sample. The sample was found to contain a small contribution of barium oxide (BaO), with a weight fraction of approximately 3.1 %. Initially there were small misfits in intensity in the longer *d*-spacing regions. Both refining the occupancies of the deuterium atoms, or mixing hydrogen/deuterium on the *4c* sites improved the fits substantially. This suggests either an approximate 7% hydrogen content in the sample or, as is more likely due to the high purity of deuterium used in

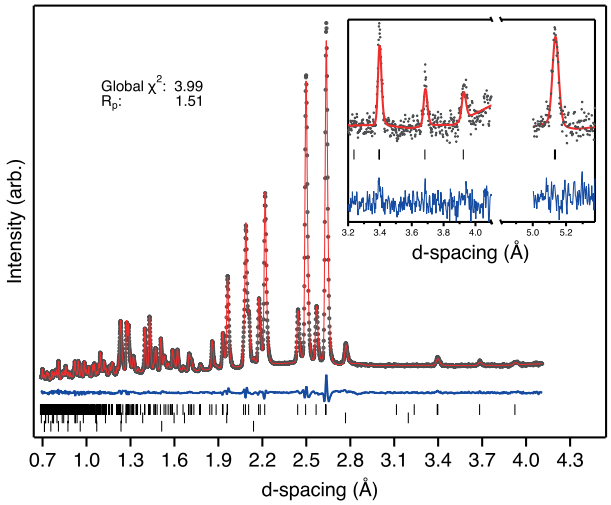

Figure 2: Powder neutron-diffraction data from the PEARL instrument, with the sample loaded into a 6 mm diameter vanadium can. The black markers represent measured data points, the solid red line (colour online) is a Rietveld fit to the data, and lower solid blue line is the residual of the fit. The upper tick marks index BaD_2 with symmetry *Pnma*, the middle tick marks are from BaO, and the lower tick marks are from vanadium. Inset: expanded region of fit to sample peaks at longer *d*-spacing range, and data fitted to the long-frame data from PEARL (see instrument details in [12]), tick marks here are only from BaD_2.

Table 1
Refined structural parameters from *Pnma* structure of BaD_2 at ambient temperature and pressure. All of the atoms are on 4c Wyckoff positions, (x,¼, z). Note that the coordinate data have been presented with a (½,½,½) origin shift so as to be comparable to those presented by Verbraeken et al. [2]. The geometry optimised structure, used for the DFT calculations, is also presented.

	Present study	Ref [2]	Present study DFT calc.
a–axis (Å)	6.78727(11)	6.7824(1)	6.82699
b–axis (Å)	4.16989(6)	4.1605(1)	4.15144
c–axis (Å)	7.84757(12)	7.8432(6)	7.85123
Volume (Å^3)	222.103(6)	221.322(6)	222.518
Ba–x	0.2395(2)	0.2393(3)	0.239267
Ba–z	0.11059(13)	0.1112(2)	0.112951
D1–x	0.35293(14)	0.3514(2)	0.355759
D1–z	0.4257(2)	0.4282(2)	0.428756
D2–x	0.9737(2)	0.9733(2)	0.971007
D2–z	0.68285(12)	0.6828(2)	0.679560
D1 Occ	0.926(2)	0.928(2)	1
D2 Occ	0.912(2)	0.911(6)	1
ρ (g cm^{-3})	4.223	-	-

the synthesis, a deuterium deficiency, resulting in a true stoichiometry of $BaD_{1.78}$ (see Figure 2). This is commonly observed in hydride materials due to the high partial hydrogen pressures required for complete synthesis, and their metastability upon removal from a hydrogen atmosphere [19]. Table 1 shows a summary of the refined model to the data (a full table of the refined model details is provided in the Supplementary Information, SI), which compare favourably [1] with those reported by Verbraeken et al. [2], and are equivalent and comparable to those reported elsewhere for BaD_2 [20, 21].

The sample was compressed isothermally at 300 K in 0.25-0.5 GPa steps up to 3.81 GPa. A transition from orthorhombic *Pnma* symmetry to hexagonal $P6_3/mmc$ symmetry was observed at approximately 2.53 GPa, with phase coexistence between the two phases observed at 2.29 GPa. The sample was then heated, and the pressure drifted from 3.8 to 5.5 GPa; the pressure was then isothermally released at 480 K. The sample was observed to transform back to the ambient pressure structure in the range 1.1-2 GPa at 480 K. The high-pressure data are summarised in Figure 3, and the refined parameters are summarised in the SI. The volume reduction through the phase transition is approximately 6.4%, with phase coexistence confirming the first order nature of the transition. Note that some hysteresis was observed on downloading the sample, with the sample transforming back to the α-phase at approximately 1.65 GPa. The shift in transition pressure with temperature from the two points determined here, and the ambient pressure transformation temperature reported in the literature [2], were fitted to a linear function. The Clausius-Clapeyron equation was then used to yield an entropy change of 34.9(5) J mol^{-1} K^{-1} for the transition. We observe a large upwards shift in the transformation pressure compared with that reported for BaH_2 [10] (1.6 GPa $\rightarrow$ 2.53 GPa), which is presumably due to a reduced mobility of deuteride ions.

The α-phase was found to compress anisotropically, with the *a*-axis being almost twice as compressible, 15.2(2) TPa^{-1}, as the other *b*- and *c*–axes which had comparable compressibilities, 7.2(4) TPa^{-1} and 7.8(3) TPa^{-1} respectively. This is consistent with the strong ionic nature of the material; the Ba cations are coplanar with the D ions on the {010} planes, such that the dense occupation of this plane makes it quite incompressible despite having the longest Ba–Ba cation separation. The *b*–axis has a shorter Ba–Ba cation separation than the *a*–axis, such that the latter is the most compressible.

With continued increase in applied pressure, the Ba–Ba ionic separation is further reduced, leading to a change in the symmetry of the lattice initiated by ionic repulsion. The separation along the *b*-axis (of the ambient pressure structure) in this new symmetry is allowed to relax, increasing from 4.107 to 4.368 Å, a ~6% increase through the transition. Similarly, within the (100)-plane, the separations change from 2× 4.107, and 4× 4.375 Å to a value of 6× 4.368 Å, showing an average increase of ~2%. This relaxed arrangement of Ba in the β-phase is accommodated by the compression of the *a*-axis and the delocalisation of the D1 ions, splitting

[1] Note a (½,½,½) origin shift from the standardised form, this convention has been kept throughout for ease of comparison with the most recent literature values.

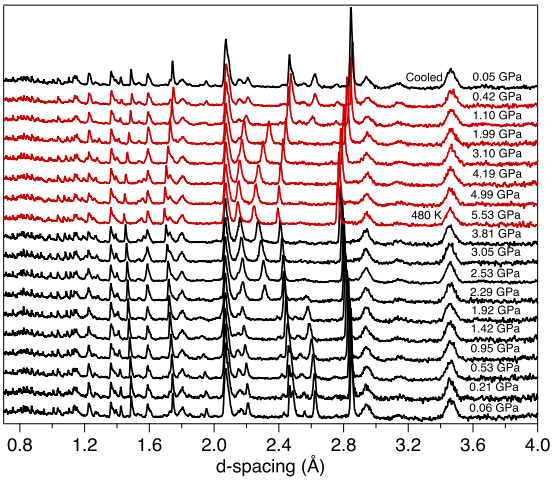

Figure 3: Compiled high-pressure neutron diffraction data (colour online). The sample was observed to fully transform by approximately 2.5 GPa at 300 K at room temperature, with phase coexistence observed at approximately 2.3 GPa consistent with a first order transition. The peaks at 2.4 and 2.85 Å are from the Pb pressure marker, the peak at 2.08 Å and dominant peaks above 2.85 Å are from the alumina, and zirconia present in the anvils. The pattens in red (colour online) were collected at 480 K.

with a partial occupancy on the 4f Wyckoff sites, see Figure 1(ii), also see SI. This results in highly mobile H^-, causing a sharp increase in the electrical conductivity of the sample as reported previously both at high temperature [2] and under applied pressure at room temperature [3]. It is also of interest to reconsider the effects of isotope enrichment in this sample, as it is to be expected that H ions are more electronically mobile than D ions, following classical theory ($\propto 1/\sqrt{m}$) as is seen elsewhere [22]. Assuming a similar thermodynamic trend for a fully hydrogenated sample, and taking the temperature of transformation as the temperature midway between phase appearance and phase purity, we can predict that BaH_2 will transform at ambient pressure at approximately 652(13) K, in reasonable agreement with the conductivity measurements reported for the fully hydrogenated sample [2]. This suggests that the entropy change is not significantly altered with isotope substitution.

The volume-pressure relation was fitted using a second-order Rydberg-Vinet equation of state (i.e $B' = 4$), the fits are shown in the SI, the α-phase was determined to have $B_0 = 29(1)$ GPa, $V_0 = 222.1(3)$ Å^3, in excellent agreement with the ambient pressure volume determined from the vanadium can data (see Table 1). At the phase transition there is an effective reduction in volume of ≈6.2%. The β-phase was fitted with $B_0 = 27.8(8)$ GPa, $V_0 = 103.9(2)$ Å^3 at 300 K and $B_0 = 25.9(3)$ GPa, $V_0 = 105.82(12)$ Å^3 at 480 K. This yields a temperature dependence of the isothermal bulk modulus of $-0.011(5)$ GPa K^{-1} for the high pressure β-phase. Attempts to fit with a third-order equation of state to the α-phase yielded a close to zero value of B', this is perhaps due to a slight softening in the curve at the point of phase coexistence; fitting over a narrower pressure range was insufficient to accurately fit the curvature.

The refined atomic positions for the α-phase show that the D1 and Ba atoms move negligibly (outside of the experimental uncertainty) from the ambient pressure positions prior to the transition (values reported in the SI). The thermal displacement parameters were fixed during the refinements, due to limitations in the data quality. The majority of the unit-cell compression is accommodated through movement of the D2 atoms (see Figure 4). Within the *ac*–plane these have the largest Ba-D separations; 2.7980(16) Å for D2 compared with 2.5976(17), 2.6400(17) Å for D1. The D2 atoms also sit in larger void sites between the trigonal faces of the zigzag chains, each coordinated to four Ba atoms rather than five (see Figure 1), and so are expected to be minimally constrained compared with D1.

In the β-phase, the D1 atoms are constrained by symmetry within the *ab*–plane of the hexagonal cell, but are seen to shift almost linearly parallel to **c** (see inset Figure 4). A shift in $D1_z$ towards $^3/_4$ indicates that the deuterium atoms become more crystallographically localised along the *c*-axis with increased pressure in the β-phase. When coupled with the reduction in cell volume the D2–D2 separation reduces significantly, whereas the D1–D2 separation is within error unchanged. If the ionic migration path is assumed to be *parallel* to the (002)-plane, D2 migration mediated by D1 vacancies, then this localisation should have little effect on the conductivity. DFT modelling shows that increased pressure reduces the hopping barrier energy for D2 along a shorter migration path *perpendicular* to the (002)-plane, resulting in an increase in ionic conductivity (using the 2d-model), confirmed with high-pressure impedance spectroscopy measurements [3]. The onset of this increase in conductivity appears approximately 2 GPa higher in pressure than the reported change in symmetry, and plateaus around 6 GPa, showing a much less pronounced increase beyond this. This coincides approximately with the pressure at which D1 is most localised according to the present study, suggesting that a gradual shift from a half occupied 4f-model to a fully occupied 2d-model is responsible for the initial large increase in conductivity, while the increase beyond this is due to a reduction in D–D separation. Zhang et al. [3] don't discuss the potential effects of the D1 localisation on the hopping energy, but they do show that the change in ionic conductivity onset with pressure at ambient temperature is gradual. This is consistent with the gradual change observed in the present study, but inconsistent with observations at ambient pressure showing the onset change in conductivity with heating as almost discontinuous, which may be due to enhanced diffusion between layers.

Tse et al. [11] inferred from the structure of hexagonal BaF_2 that the β-phase of BaH_2 had hydrogen positions on the 2a and 2d Wyckoff sites. Verbraeken et al. [2] showed that it is in fact very difficult to distinguish whether the hydrogen is on the 2d site, or partially occupied on the 4f site, from diffraction data. This was due to the large thermal anisotropy for the 2d-model ($U_{33}^{\text{D1 on 2d}} \approx 0.47$), which essentially por-

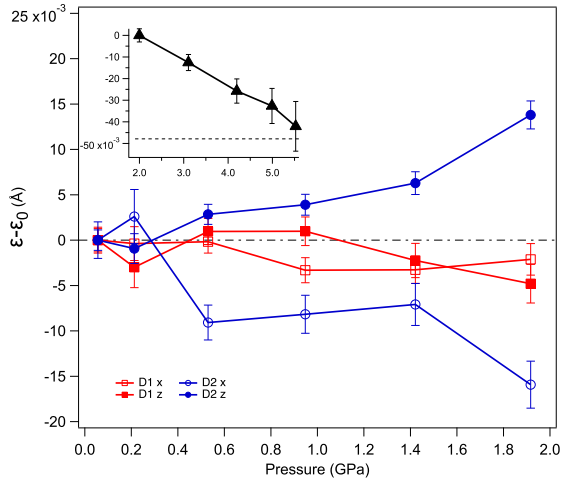

Figure 4: Relative change in deuterium coordinates (where $\epsilon = x, y, z$) of the α-phase as a function of pressure at 300 K. Inset: β-phase deuterium position (D1 z) at 480 K collected on pressure decrease, showing a linear shift towards the $^3/_4$ 2d-Wyckoff position (dashed line represents shift required to reach $z = {}^3/_4$) at higher pressures.

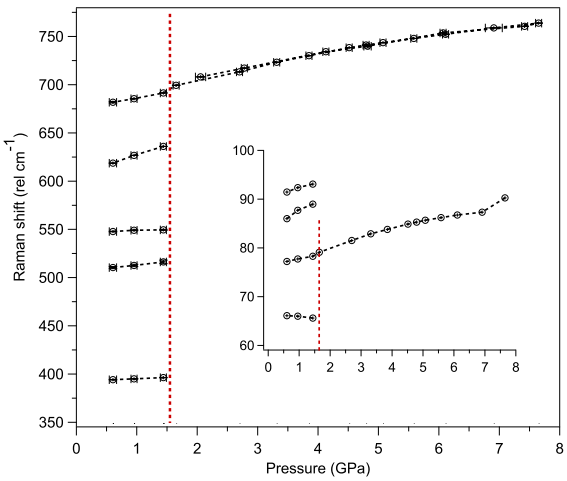

Figure 5: Shift of the fitted Raman modes as a function of pressure, a clear change in the number of peaks present is seen upon symmetry change at approximately 1.5 GPa on downloading. Inset: expanded region around the low energy Ba dominated modes.

trays the two models as equivalent. When the changes in the deuterium positions are considered leading up to the transition (also see Figure 1), it is clear that the shift of D1 from 4c in the orthorhombic structure to 4f in the hexagonal structure is very subtle if thermal motion along the c-axis is considered. Our data are insufficient to distinguish between the 4f- and 2d- models at the point of the transition, but where the 4f-model is assumed, and the thermal displacement parameters are fixed, a shift towards the 2d-model is observed with increased pressure.

3.2. Raman spectroscopy

The expected Raman-active irreducible representations (irreps) for the α-phase are $\Gamma_{Pnma} = 6A_g + 3B_{1g} + 6B_{2g} + 3B_{3g}$, and with an increase in symmetry the number of modes lowers to $\Gamma_{P6_3/mmc} = 2E_g$ for the β-phase. Spectra were collected on pressure increase, and on decrease (see SI for raw spectra, fitted peak positions shown in Figure 5). On increasing the pressure to approximately 2.3 GPa, the number of modes present in the spectra changed as expected, confirming that the sample was in the β-phase, consistent with the neutron data. This was found to be reversible upon releasing the pressure to approximately 1.6 GPa.

The positions of the CASTEP calculated Raman modes are in very good agreement with those observed experimentally, see Table 2 for a comparison between the two, and their symmetry assignments, though it was either not possible to fully resolve all of the modes experimentally, or they were too weak to observe. The modes up to approximately 150 rel cm^{-1} are predominantly due to the Ba ion vibrations, and those beyond this are dominated by the deuterium ion vibrations. The majority of the observed modes are observed to 'harden' to higher energies with increased pressure, as expected from Grüneisen theory, though the lowest energy mode observed at approximately 65 rel cm^{-1} is seen to soften over the observed pressure range. This mode is dominated by the out of phase motion of the two closest Ba atoms, along the b- and c- axes of the crystallographic unit-cell (see schematic in SI). Since the unit-cell is significantly less compressible along these two axes due to shorter Ba-Ba distances, this soft-mode appears to drive the first-order displacive phase transition to the hexagonal structure. It is possible that previous measurements did not observe this effect due to a limited number of data points in the low pressure phase [10]. The intensity of the mode observed at approximately 77 rel cm^{-1} (assigned to the B_{1g} symmetry) is also observed to change significantly relative to all the other modes in this region. This would suggest that there is an increase in the polarisability of this mode, consistent with the β-phase being a more planar structure (along the b-axis). This would then suggest that it is the out-of-phase motion of the Ba atoms along the b-axis which is observed to soften rather than the B_{3g} mode.

4. Conclusion

The α- and β-phases of BaD_2 have been studied as a function of pressure and temperature using neutron diffraction and Raman spectroscopy, providing the first detailed structural analysis (including deuterium positions) of this material at high pressure. The compression of the α-phase shows that the ionic nature of the material results in a highly compressible a-axis, which is accommodated by the movement of the D2 atoms, leaving the Ba and D1 atoms essentially unchanged. The transition to the β-phase allows for the Ba–Ba separations to on average increase by 2% within the (100)-plane, and 6% along the b-axis, through delocalising the D1 atoms. Raman spectroscopy shows a gradual softening of a low-energy mode leading up to the first-order

Table 2
Symmetry mode (irrep) assignments from CASTEP finite-displacement calculations, compared with the modes observed experimentally at ambient pressure and temperature for the *Pnma* phase. The assignments are provided to give an indication of the dominant atomic motions contributing to each mode, the atom is labelled with + for in-phase, and − for out-of-phase motion between nearest atoms, along a specified crystallographic axis. For full details, the phonon eigenvectors are provided in the SI.

CASTEP calculated (rel cm^{-1})	Irrep.	Assign.	Experiment (rel cm^{-1})
65.4	B_{3g}	Ba_b^-	
66.6	A_g	Ba_c^-	66.101(11)
82.4	B_{1g}	Ba_b^+	77.21(18)
90.9	A_g	Ba_a^+	85.99(14)
107.3	B_{2g}	Ba_b^+	91.46(5)
123.8	B_{2g}	Ba_a^-	
362.9	B_{1g}	$D2_b^+$	
364.7	A_g	$D2_c^-$	
390.5	B_{3g}	$D2_b^-$	394.2(2)
406.4	A_g	$D2_c^-$	
420.2	B_{2g}		
476.9	B_{2g}		
523.6	B_{2g}	$D1_a^-$	510.4(1.1)
535.6	A_g		
558.0	B_{1g}	$D1_a^+$	547.8(3)
585.5	A_g		
586.6	B_{3g}	$D1_b^-$	618.63(10)
649.1	B_{2g}	$D1_c^+$	681.8(7)

transition, which DFT calculations indicate is dominated by the motion of the Ba atoms along the *b*- and *c*-axes, which could suggest that this soft-mode drives the transition to the β-phase. The position of the D1 atom upon continued increase in pressure was determined to localise towards the value expected for a localised 2d-Wyckoff position. This appears to be in agreement with literature reports of high-H^- ionic conductivity in BaH_2 under high-pressure, explained assuming a migration path perpendicular to the (002)-plane, and could explain the plateau in the conductivity curve as a function of pressure.

Acknowledgments

The authors acknowledge the Science and Technology Facilities Council (STFC) for providing access to the PEARL instrument at the ISIS Neutron and Muon Source [23]. The authors wish to thank Elisabeth Lindner for assisting in preparing the sample. The authors also wish to thank Paul Henry for his assistance in sourcing the sample. Computing resources were provided by the STFC Scientific Computing Department's SCARF cluster.

References

[1] J. Andersson, S. Grönkvist, Large-scale storage of hydrogen, International Journal of Hydrogen Energy 44 (2019) 11901 – 11919.
[2] M. C. Verbraeken, C. Cheung, E. Suard, J. T. S. Irvine, High H^- ionic conductivity in barium hydride, Nature Materials 14 (2015) 95.
[3] X. Zhang, X. Wang, Q. Wang, X. Ma, C. Liu, P. Li, C. Liu, Y. Han, Y. Ma, C. Gao, Hydride ion (H^-) transport behavior in barium hydride under high pressure, Phys. Chem. Chem. Phys. 20 (2018) 8917–8923.
[4] K. Fukui, S. Iimura, T. Tada, S. Fujitsu, M. Sasase, H. Tamatsukuri, T. Honda, K. Ikeda, T. Otomo, H. Hosono, Characteristic fast H^- ion conduction in oxygen-substituted lanthanum hydride, Nature Communications 10 (2019) 2578.
[5] E. Zintl, A. Harder, Constitution of alkaline earth hydrides, Zeitschrift für Elektrochemie und angewandte physikalische Chemie 41 (1935) 33–52.
[6] J. Bergsma, B. O. Loopstra, The crystal structure of calcium hydride, Acta Crystallographica 15 (1962) 92–93.
[7] D. T. Peterson, M. Indig, The barium-barium hydride phase system, Journal of the American Chemical Society 82 (1960) 5645–5646.
[8] W. Luo, R. Ahuja, Ab initio prediction of high-pressure structural phase transition in BaH_2, Journal of Alloys and Compounds 446 (2007) 405–408.
[9] K. Kinoshita, M. Nishimura, Y. Akahama, H. Kawamura, Pressure-induced phase transition of BaH_2: Post Ni_2In phase, Solid state communications 141 (2007) 69–72.
[10] J. S. Smith, S. Desgreniers, J. S. Tse, D. D. Klug, High-pressure phase transition observed in barium hydride, Journal of Applied Physics 102 (2007) 043520.
[11] J. S. Tse, Z. Song, Y. Yao, J. S. Smith, S. Desgreniers, D. D. Klug, Structure and electronic properties of BaH_2 at high pressure, Solid State Communications 149 (2009) 1944–1946.
[12] C. L. Bull, N. P. Funnell, M. G. Tucker, S. Hull, D. J. Francis, W. G. Marshall, PEARL: the high pressure neutron powder diffractometer at ISIS, High Pressure Research 36 (2016) 493–511.
[13] S. Klotz, J. M. Besson, G. Hamel, R. J. Nelmes, J. S. Loveday, W. G. Marshall, R. M. Wilson, Neutron powder diffraction at pressures beyond 25 GPa, Applied Physics Letters 66 (1995) 1735–1737.
[14] T. Strässle, S. Klotz, K. Kunc, V. Pomjakushin, J. S. White, Equation of state of lead from high-pressure neutron diffraction up to 8.9 GPa and its implication for the NaCl pressure scale, Physical Review B 90 (2014) 014101.
[15] L. Merrill, W. Bassett, Miniature diamond anvil pressure cell for single crystal X-ray diffraction studies, Review of Scientific Instruments 45 (1974) 290–294.
[16] G. Piermarini, S. Block, J. Barnett, R. Forman, Calibration of the pressure dependence of the R1 ruby fluorescence line to 195 kbar, Journal of Applied Physics 46 (1975) 2774–2780.
[17] S. J. Clark, M. D. Segall, C. J. Pickard, P. J. Hasnip, M. I. J. Probert, K. Refson, M. C. Payne, First principles methods using CASTEP, Zeitschrift für Kristallographie-Crystalline Materials 220 (2005) 567–570.
[18] J. P. Perdew, K. Burke, Y. Wang, Generalized gradient approximation for the exchange-correlation hole of a many-electron system, Physical Review B 54 (1996) 16533.
[19] Y. Zhang, M. C. Verbraeken, C. Tassel, H. Kageyama, Metal hydrides, Handbook of Solid State Chemistry (2017) 477–520.
[20] W. Bronger, S. Chi-Chien, P. Müller, The crystal structure of barium hydride, determined by neutron diffraction experiments on BaD_2, Zeitschrift für Anorganische und Allgemeine Chemie 545 (1987) 69–74.
[21] G. J. Snyder, H. Borrmann, A. Simon, Crystal structure of barium dihydride, BaH_2, Zeitschrift fur Kristallographie 209 (1994) 458–458.
[22] S. Shioya, T. Nagasaki, T. Matsui, H. Shigematsu, Lithium-isotope effect on ionic conductivity of $(La_{0.5}Li_{0.27})_{0.95}Sr_{0.05}TiO_{2.92}$, Solid State Ionics 161 (2003) 55–59.
[23] C. J. Ridley, N. P. Funnell, C. L. Bull, STFC ISIS Facility data, 2018. https://doi.org/10.5286/ISIS.E.RB1810432.

Supplementary Information

Neutron diffraction study of the α- to β- phase transition in BaD_2 under high pressure

Christopher J. Ridley[a], Nicholas P. Funnell[a], Craig L. Bull[a] and Holger Kohlmann[b]

[a] *ISIS Neutron and Muon Source, Rutherford Appleton Laboratory, Chilton, Didcot OX11 0QX, United Kingdom*
[b] *Institut für Anorganische Chemie, Universität Leipzig, Johannisallee 29, 04103 Leipzig, Germany*

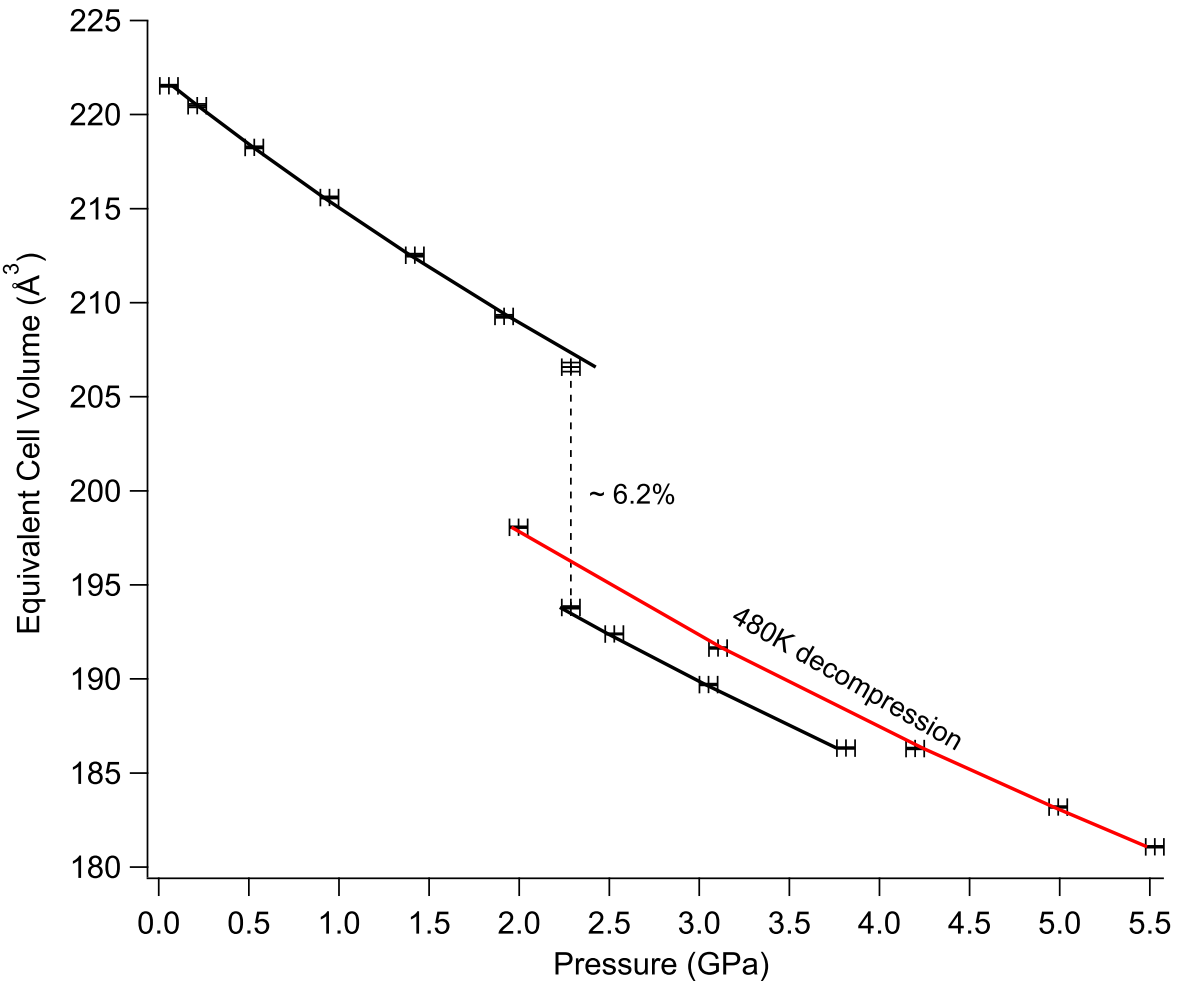

Figure S1: Compiled Volume-Pressure data for the α- and β-phases at $300\,\mathrm{K}$, and $480\,\mathrm{K}$ as indicated, with fitted equation of states as discussed in the main text. The volume of the β-phase (Z=2) is multiplied by two to allow a direct comparison with the α-phase (Z=4).

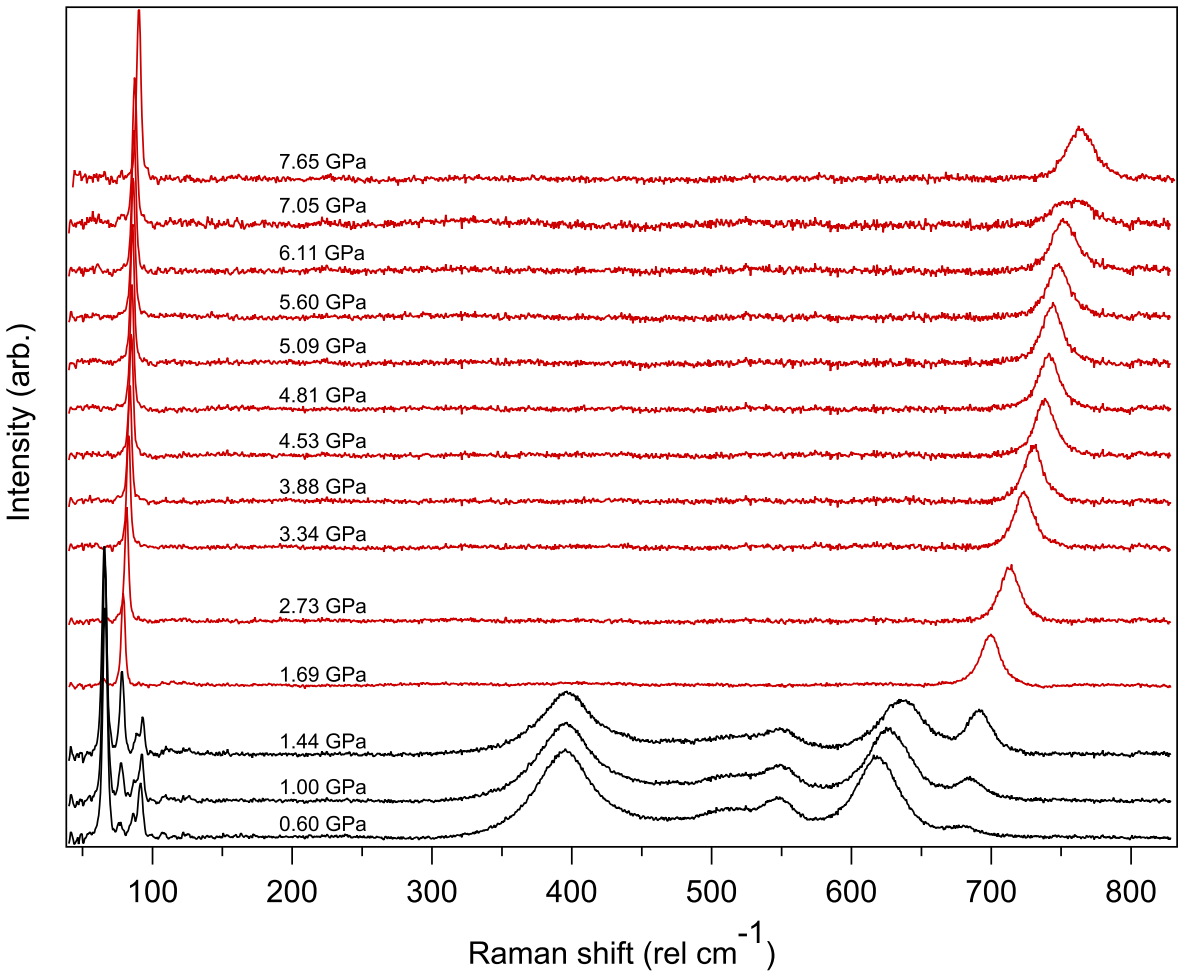

Figure S2: Compiled high-pressure Raman spectra in agreement with the predicted lowering of vibrational modes allowed by symmetry through the transition from orthorhombic to hexagonal symmetry.

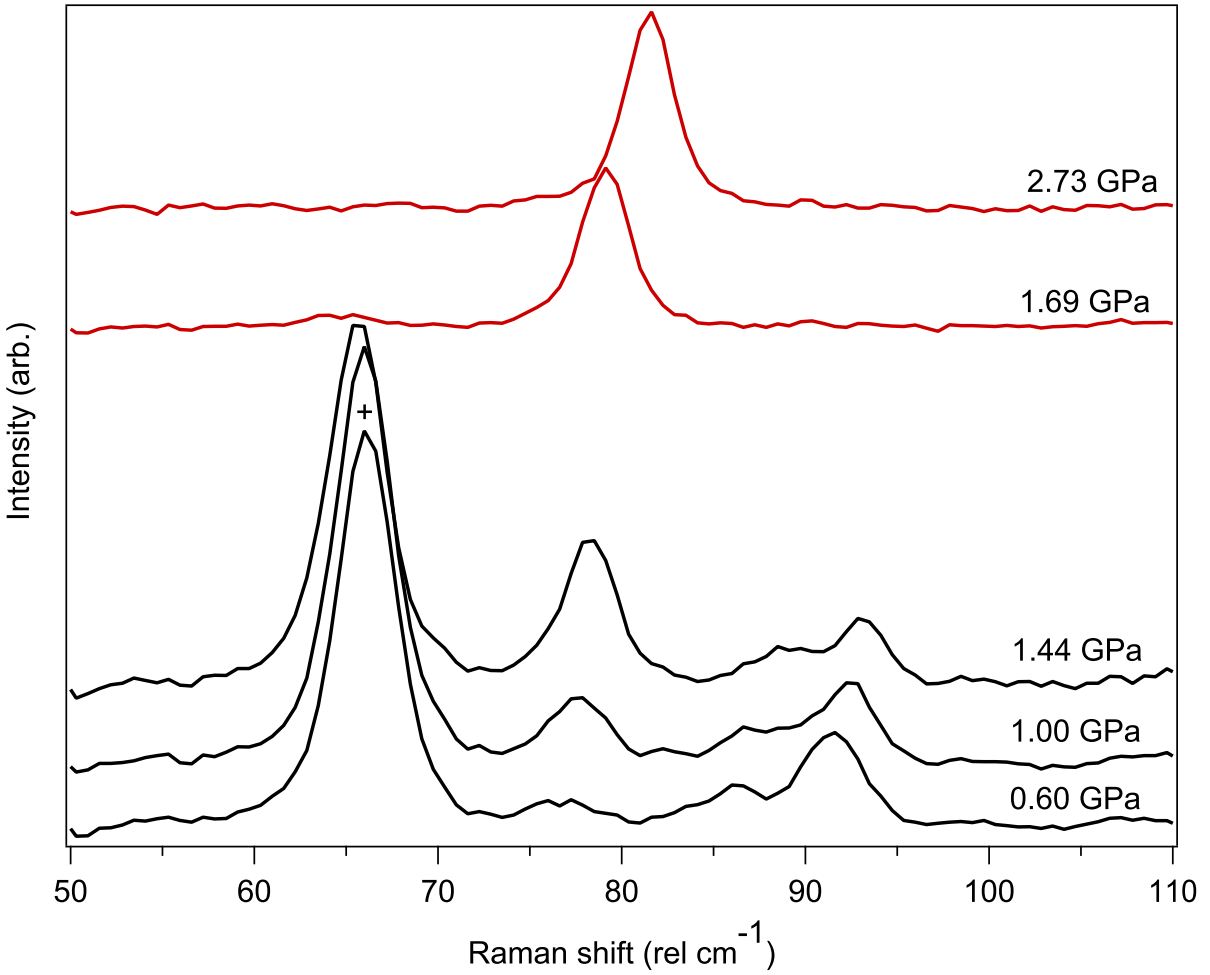

Figure S3: Exploded low-energy region of the Raman spectra under applied pressure showing the softening of B_{3g}/A_g modes corresponding to the barium out-of-phase oscillations along the b- and c-axes respectively, as indicated by +.

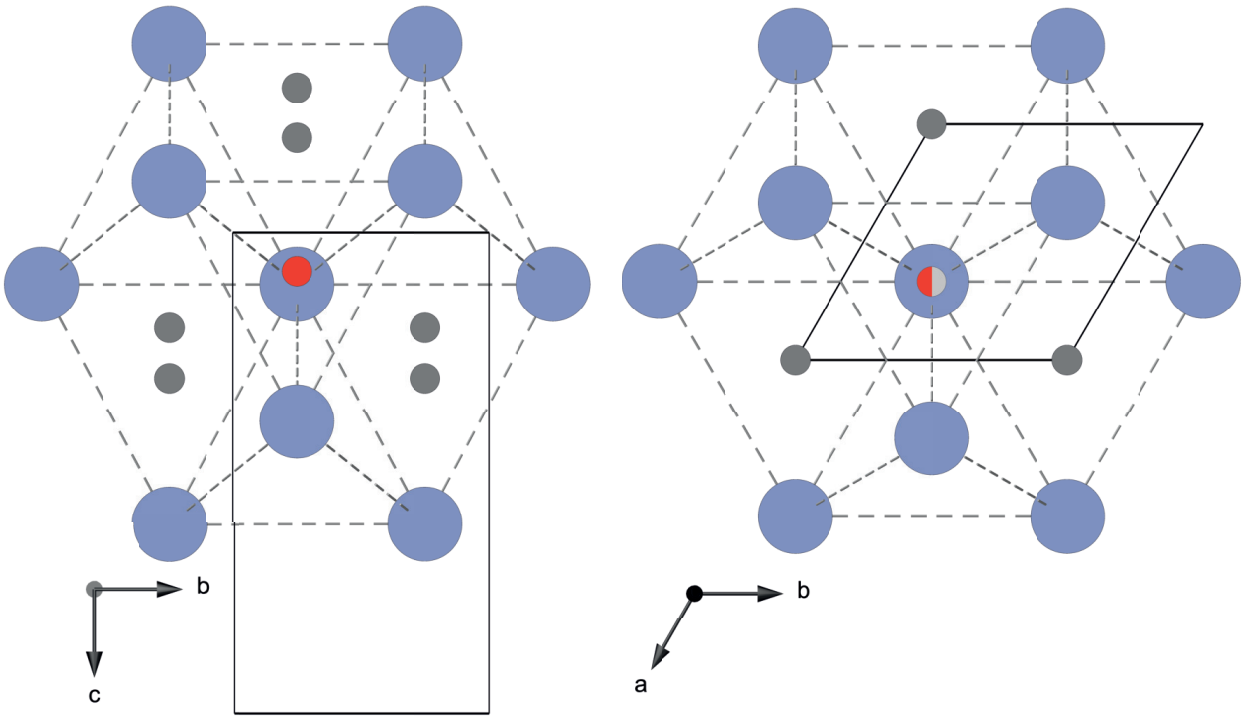

Figure S4: Side-by-side structures of the α-phase at 1.92(5) GPa prior to the transition as viewed along the [100] direction (left), and the β-phase at 2.53(5) GPa post the transition (right). The β-phase is viewed along the [001] direction, with the partially occupied deuterium ion sites shown as half-shaded circles.

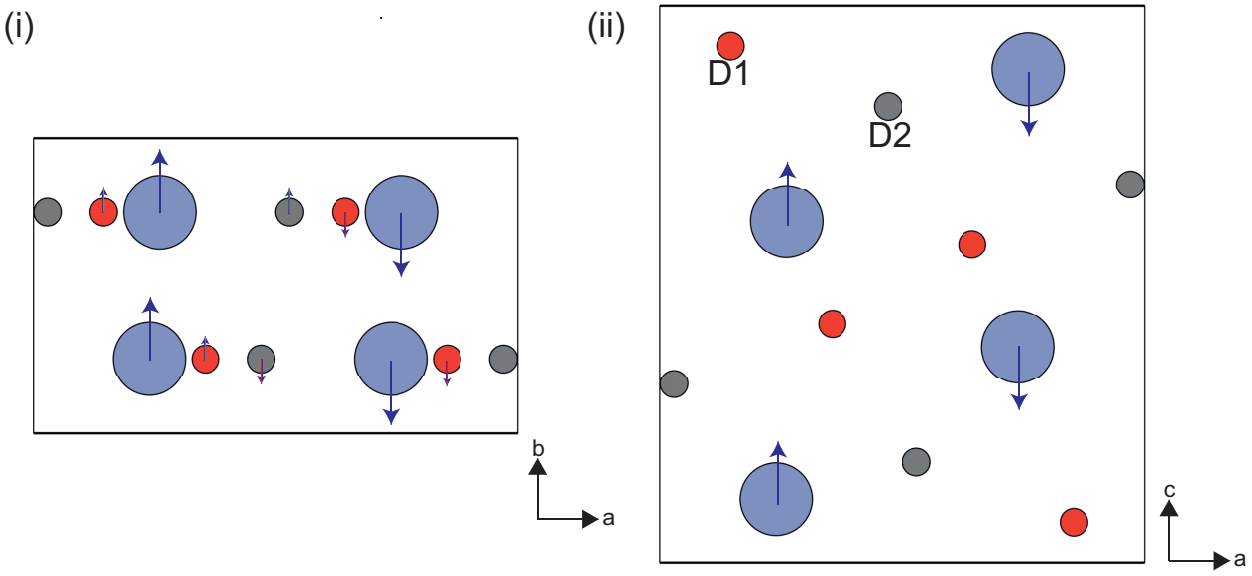

Figure S5: (Schematic showing the dominant atomic motions, contributing to the Raman active mode observed to soften prior to the phase transition. As determined by the DFT calculations. (i) 65.4 rel cm^{-1} mode as viewed in *ab*-plane, (ii) 66.6 rel cm^{-1} mode as viewed in *ac*-plane.

Table S1

Full list of refined parameters from *Pnma* structure of BaD_2 at 300 K, and 100 K, at ambient pressure from the present study. All of the atoms are on 4c Wyckoff positions, (x,¼, z). Note that the coordinate data have been presented with a (½,½,½) origin shift. The 100 K data were collected in a 100 mm diameter orange cryostat with a vanadium heat-shield, while the ambient temperature data were collected outwith of the cryostat in a low background aluminium vacuum tank. As such the refined occupancies were fixed to the ambient temperature values for the cryostat measurements. The 300 K dataset was collected over a period of 17 h in 1 h intervals; no changes were observed in the pattern during this time. Similarly, diffraction data were compared over each of the nine separate $2\theta = 90°$ detector banks, and no differences in peak intensities were observed, suggesting no texture or preferred orientation in the sample.

Temperature	300 K	100 K
a–axis (Å)	6.78727(11)	6.77909(13)
b–axis (Å)	4.16989(6)	4.15585(7)
c–axis (Å)	7.84757(12)	7.84500(15)
Volume (Å^3)	222.103(6)	221.016(7)
Ba–x	0.2395(2)	0.2401(3)
Ba–z	0.11059(13)	0.11191(14)
β_{11}^{Ba}, β_{22}^{Ba}	31(3), 183(7)	24(4), 59(8)
β_{33}^{Ba}, β_{13}^{Ba} ($\times 10^4$)	25(2), 1(2)	19(3), 5(2)
D1–x	0.35293(14)	0.35356(15)
D1–z	0.4257(2)	0.42736(16)
β_{11}^{D1}, β_{22}^{D1}	112(4), 222(9)	77(4), 205(11)
β_{33}^{D1}, β_{13}^{D1} ($\times 10^4$)	70(2), 11(2)	45(3), 2(2)
D2–x	0.9737(2)	0.9712(2)
D2–z	0.68285(12)	0.68245(13)
β_{11}^{D2}, β_{22}^{D2}	139(4), 299(9)	111(4), 254(11)
β_{33}^{D2}, β_{13}^{Ba} ($\times 10^4$)	130(3), 5(3)	94(3), -11(3)
D1 Occ	0.926(2)	-
D2 Occ	0.912(2)	-
ρ (g cm^{-3})	4.223	4.234
R_p	6.47	7.65
R_{wp}	5.63	5.90
R_{exp}	2.08	3.49
χ^2	7.34	2.87

Table S2
Crystallographic data for the 300 K compression of the α-phase of BaD_2 determined form Rietveld analysis of the PEARL neutron powder diffraction data. All refinements performed using the *Pnma* orthorhombic space-group with Ba: 4c $(x, 1/4, z)$, D1: 4c $(x, 1/4, z)$, D2: 4c $(x, 1/4, z)$. The atomic coordinates were not refined for the 2.29 GPa mixed phase pressure point, due to instability, and are therefore omitted. The occupancies of the D1 and D2 sites were fixed to that determined from the vanadium can data, 0.926 and 0.912 respectively.

Pressure (GPa)	0.06(5)	0.21(5)	0.53(5)	0.95(5)	1.42(5)	1.92(5)	2.29(5)
a–axis (Å)	6.7891(10)	6.7758(16)	6.7418(9)	6.6967(11)	6.6525(14)	6.6008(16)	6.565(5)
b–axis (Å)	4.1610(7)	4.1555(10)	4.1472(6)	4.1396(7)	4.1211(8)	4.1067(9)	4.083(2)
c–axis (Å)	7.8419(11)	7.8301(17)	7.8062(10)	7.7768(12)	7.7521(15)	7.7204(16)	7.707(5)
V_{cell} (Å^3)	221.53(6)	220.47(9)	218.26(5)	215.59(6)	212.53(8)	209.28(8)	206.6(2)
Ba x	0.2333(17)	0.238(3)	0.2367(17)	0.2311(17)	0.2333(19)	0.238(2)	-
Ba z	0.1074(13)	0.103(2)	0.1061(13)	0.1043(15)	0.1021(18)	0.107(2)	-
D1 x	0.3510(13)	0.3506(19)	0.3508(13)	0.3476(14)	0.3477(15)	0.3488(17)	-
D1 z	0.4251(14)	0.422(2)	0.4260(14)	0.4260(16)	0.4228(19)	0.420(2)	-
D2 x	0.982(2)	0.985(3)	0.9731(19)	0.974(2)	0.975(2)	0.966(3)	-
D2 z	0.6835(11)	0.6825(17)	0.6864(11)	0.6875(12)	0.6898(13)	0.6974(15)	-
χ^2	0.98	0.64	1.10	0.90	0.91	0.94	0.86
wRp	4.41	6.51	4.30	4.41	4.50	4.58	4.44

Table S3
Crystallographic data for the compression (at 300 K) and decompression (at 480 K) of the β-phase of BaD_2 determined form Rietveld analysis of the PEARL neutron powder diffraction data. All refinements performed using the $P6_3/mmc$ hexagonal space-group with Ba: 2b $(1/3, 2/3, 1/4)$, D1: 4f $(1/3, 2/3, z)$, D2: 2a $(0, 0, 0)$. The atomic coordinates were not refined for the 2.29 GPa mixed phase pressure point, due to instability, and are therefore omitted. The occupancies of D1 and D2 were initially refined and then fixed to values of 0.492 and 0.822 respectively.

Pressure (GPa)	2.29(5)	2.53(5)	3.05(5)	3.81(5)	5.53(5)	4.99(5)	4.20(5)	3.10(5)	1.99(5)
Temperature (K)	300	300	300	300	480	480	480	480	480
a–axis (Å)	4.3679(7)	4.3613(4)	4.3486(5)	4.3323(5)	4.3009(5)	4.3125(5)	4.3281(5)	4.3553(4)	4.3780(4)
c–axis (Å)	5.8649(14)	5.8398(9)	5.7918(9)	5.7316(9)	5.6518(11)	5.6871(10)	5.7422(10)	5.8332(9)	5.9662(10)
V_{cell} (Å^3)	96.90(3)	96.20(2)	94.85(2)	93.16(2)	90.54(2)	91.60(2)	93.16(2)	95.82(2)	99.03(2)
D1 z	-	0.794(2)	0.773(4)	0.764(14)	0.756(11)	0.765(8)	0.772(6)	0.785(4)	0.798(3)
χ^2	0.86	1.89	1.01	1.08	1.05	1.14	1.20	1.20	1.13
wRp	4.44	4.41	4.91	5.13	5.27	5.44	5.55	5.34	5.25